ACADEMIC PRESS

Available online at www.sciencedirect.com
SCIENCE DIRECT®

Journal of Colloid and Interface Science 257 (2003) 291–298

JOURNAL OF Colloid and Interface Science

www.elsevier.com/locate/jcis

Effect of multiple scattering on SANS spectra from bicontinuous microemulsions

James A. Silas and Eric W. Kaler *

Center for Molecular and Engineering Thermodynamics, Department of Chemical Engineering, University of Delaware, Newark, DE 19716, USA

Received 3 August 2001; accepted 4 October 2002

Abstract

Small-angle neutron scattering is a powerful tool for investigating the microstructure of self-assembled systems. The domain length, d, and the correlation length, ξ, are two measures of bicontinuous microemulsions that are often determined from coherent SANS spectra. Some microemulsions scatter strongly, however, so measured spectra can contain multiple coherent scattering, and neglect of that multiple scattering can lead to incorrect values of d and ξ. In addition, multiple scattering can give rise to artifacts in the spectra, most notably an apparent scattering peak at twice the value of the scattering vector of the main peak. Here, changes in the SANS spectra from strongly scattering microemulsions and the parameters derived from them are reported as a function of relative scattering probability by varying both sample thickness and scattering contrast. A linear extrapolation of the results to zero scattering probability yields good estimates for the microstructural parameters, and the numerical procedure of Schelten and Schmatz is used to calculate the specific effects of multiple scattering on typical bicontinuous microemulsion scattering spectra.

Keywords: Microemulsions; Multiple scattering

1. Introduction

Microemulsions are thermodynamically stable, microstructured solutions of at least surfactant, oil, and water, and are just one of many self-assembled system that have received attention in recent years [1,2]. Because of their thermodynamic stability, the structure of microemulsions is set only by their composition and temperature and is often in the range of 10 to 1000 Å. These length scales, as well as the scattering contrast available by selective deuteration of different chemical components, have made small-angle neutron scattering (SANS) an attractive tool for the investigation of microemulsion microstructure.

The coherent elastic small-angle scattering of microemulsions has been used to measure the shape, size, and other properties of surfactant microstructures under the assumption of single scattering [3–8]. However, due to the intense scattering from some bicontinuous microemulsions (transmissions $< 30\%$), some authors have reported a dependence of the small-angle scattering spectra on the sample thickness [9]. This indicates that a certain amount of multiple scattering is present within the spectra, and the purpose of this paper is to quantify and analyze the effect of multiple scattering on bicontinuous microemulsion spectra and any derived structural parameters.

There are many descriptions of multiple scattering in the literature that arrive at similar expressions for multiple elastic coherent scattering [10–16], most of which were summarized by Berk and Hardman-Rhyne [13]. Early work focuses on several approximations that are convenient for numerical calculations [10,11], while more recent results show the amount of information available in spectra as the transmission approaches zero [13], or the effect of the statistical nature of the medium on the resulting spectra [16]. Barabanov and Belyaev have recently outlined a more comprehensive approach to both coherent elastic and inelastic multiple scattering [17].

The numerical treatment proposed by Schelten and Schmatz uses multiple convolution products to describe the cascade of coherent scattering events in slices of increasing path length [12]. This numerical approach was used by Monkenbusch to develop two FORTRAN programs to convolute and deconvolute two-dimensional multiply scattered

* Corresponding author.
E-mail address: kaler@che.udel.edu (E.W. Kaler).

0021-9797/03/$ – see front matter
PII: S0021-9797(02)00059-0

data [14]. While Monkenbusch addresses the broadening of the main correlation peak in the spectra of microemulsions made with the surfactant AOT, experimental accounts also indicate that there are q dependent changes in the shape of microemulsion spectra at higher wave vector, most notably in terms of a secondary peak or shoulder in the spectra [9]. This feature is irreconcilable with current microemulsion scattering models and must be removed or accounted for to obtain reliable structural information from the scattering spectra.

The amount of multiple scattering is related to the overall probability that a neutron will scatter within a sample of given thickness. The probability, P, scales as

$$P(\text{scattering}) \propto D\frac{d\Sigma}{d\Omega}(\Delta\rho^2), \tag{1}$$

where D is the thickness and $\Delta\rho$ is the difference in scattering length density between the two bulk domains. The microstructure of the sample defines the total differential scattering cross section, $d\Sigma/d\Omega$, and so sets the q dependence when there is negligible multiple scattering. The dependence of multiple scattering on many factors including the magnitude and q dependence of the scattering cross section, the wavelength of the neutrons, and scattering angle distorts the shape of the SANS spectra so the scattered intensity no longer scales uniformly with the thickness or scattering contrast. Thus, any changes in the shape of the experimental spectra as a function of sample thickness or scattering contrast indicate significant multiple scattering is present.

This paper explores the effect of scattering contrast and path length on SANS spectra experimentally and numerically to determine the contribution of multiple scattering to the coherent elastic scattering spectra of strongly scattering bicontinuous microemulsions. The increase in the width of the correlation peak as well as the rescattering of the main correlation peak at higher q is investigated to determine the effect of multiple scattering on subsequent model fitting. SANS spectra from microemulsions at the same composition but different path lengths and contrasts demonstrate the effect of these experimental parameters. The same parameters are examined numerically through the implementation of the formalism of Schelten and Schmatz [12].

2. Materials and methods

2.1. Materials

Didodecyldimethylammonioum bromide (>99%), DDAB, was obtained from TCI America. *N*-Octyl trioxyethylene glycol ether (>99%), C_8E_3, and *n*-dodecyl trioxyethylene glycol ether (>99%), $C_{12}E_3$, were obtained from Nikko. Decane (>98%) was purchased from Fluka. Water was filtered through a 0.2-μm filter, distilled, and deionized until the specific resistance was 18.3 MΩ cm. D_2O (99.9%, DLM-11) was obtained from Cambridge Isotopes. All materials were used without further purification.

2.2. Phase behavior determination

For a four-component mixture composed of water (A), oil (B), nonionic surfactant (C), and ionic surfactant (D) the phase space is defined by temperature, pressure, and three composition variables. The mass fraction of oil on a surfactant-free basis, α, is defined as

$$\alpha = \frac{B}{A+B} \times 100, \tag{2}$$

the mass fraction of surfactant, γ, is defined as

$$\gamma = \frac{C+D}{A+B+C+D} \times 100, \tag{3}$$

and the mass fraction of ionic surfactant in the surfactant mixture, δ, is defined as

$$\delta = \frac{D}{C+D} \times 100. \tag{4}$$

For a ternary mixture, $\delta = 0$.

Sections at $\alpha = 50$ are used to determine the least amount of surfactant needed to solubilize equal weights of oil and water. This occurs at the "x-point", where the one- and three-phase microemulsions meet at a point at $\alpha = 50$, and has the coordinates of $\gamma = \tilde{\gamma}$ and $T = \tilde{T}$. The amount of surfactant at the x-point, $\tilde{\gamma}$, is the efficiency of the surfactant being measured. The replacement of H_2O with D_2O generally lowers phase boundaries by about 2°. The phase behavior of solutions with both isotopes was measured using the procedures originally developed by Kahlweit to determine the one-phase regions to be subsequently investigated with SANS [18,19].

2.3. Neutron scattering

Experiments were performed on a 30 m spectrometer at the National Institute of Standards and Technology Cold Neutron Research Facility (NIST-CNRF) in Gaithersburg, MD. Neutrons of $\lambda = 6$ Å with $\Delta\lambda/\lambda = 11\%$ were collimated and focused on thermally equilibrated one-phase samples held in quartz cells. Detector distances of 1, 4.5, and 13 m were used to obtain spectra over q-values from 0.004 to 0.5 Å^{-1}. The detector was offset 25 cm for detector distances of 1 and 4.5 m to provide adequate overlap for combining data sets. Scattering spectra were corrected using standard procedures for background, empty cell scattering, and detector sensitivity. Before model fitting, the incoherent background was determined and removed from the spectra by means of a Porod plot [20]. Samples were placed on an absolute scale using standards provided by NIST, but the absolute scaling of the model fit is not used, as described below.

3. Neutron scattering theory

3.1. Bicontinuous microemulsion scattering

The Teubner and Strey phenomenological model often accurately describes scattering from bicontinuous microemulsions [3]. The scattered intensity for this model is

$$I_{\mathrm{TS}}(q) = \frac{8\pi c_2 \langle \eta^2 \rangle / \xi}{a_2 + c_1 q^2 + c_2 q^4}, \tag{5}$$

where $\langle \eta^2 \rangle \equiv \phi_{\mathrm{o}} \phi_{\mathrm{w}} \langle \Delta\rho^2 \rangle$ and $\langle \Delta\rho^2 \rangle$ is the difference in scattering length density between oil (o) and water (w). This corresponds to an isotropic real space correlation function, $\gamma(r)$, that incorporates alternating regions of water and oil,

$$\gamma(r) = \frac{\sin(kr)}{kr} \exp\left(-\frac{r}{\xi}\right), \tag{6}$$

where $k = 2\pi/d$. The two length scales in the solution, d and ξ, are related to a_1, c_1 and c_2 via

$$\frac{d}{2\pi} = \left[\frac{1}{2}\left(\frac{a_2}{c_2}\right)^{1/2} - \frac{c_1}{4c_2}\right]^{-1/2}, \tag{7}$$

$$\xi = \left[\frac{1}{2}\left(\frac{a_2}{c_2}\right)^{1/2} + \frac{c_1}{4c_2}\right]^{-1/2}. \tag{8}$$

The length scale d represents a quasiperiodic repeat distance between water and oil regions within the solution, while the correlation length, ξ, corresponds to a characteristic length for positional correlation.

Microemulsion structure ranges from completely disordered solutions to the macroscopic ordering of a lamellar phase. An amphiphilicity factor, f_a, can be defined as [21,22]

$$f_a = \frac{c_1}{(4a_2c_2)^{1/2}}. \tag{9}$$

The value of f_a ranges from 1 for a completely disordered solution to -1 for a lamellar phase. The Lifschitz line is crossed when $f_a = 0$, and at this point a peak in the scattering spectra is observed at nonzero wave vector. The amphiphilicity factor provides a useful scale for the quantification of ordering in microemulsions.

3.2. Multiple elastic scattering

Schelten and Schmatz showed that the observed scattering pattern for elastic coherent scattering, or true scattering probability, $H(q)$, depends on the scattering cross section, $S(q)$, via [12]

$$H(q) = \frac{\Delta I}{I_0 \Delta\Omega} = k_0^2 e^{-\mu D} \sum_{n=1}^{\infty} \left(k_0^{-2}\right)^n \frac{[{}^*S(q)]^n}{n!}, \tag{10}$$

where I_0 is the primary beam intensity, μ is an attenuation coefficient, D is the sample thickness, and k_0 is the wavenumber of the incident radiation. $[{}^*S(q)]^n$ is the n-times convolution of $S(q)$ with itself according to

$$\left[{}^*S(q)\right]^2 = \int S(\xi_1) S(q - \xi_1)\, d\xi_1,$$

$$\left[{}^*S(q)\right]^3 = \int S(\xi_1) S(\xi_2 - \xi_1) - S(q - \xi_2)\, d\xi_1\, d\xi_2. \tag{11}$$

For $n = 1$, $H(q) = e^{-\mu D} S(q)$. The attenuation factor μ includes attenuation by absorption and any scattering, but here all forms of attenuation other than small angle scattering are ignored. This assumption limits the following treatment by removing the absolute scale from the model calculations.

To calculate the effects of multiple scattering for the Teubner–Strey $S(q)$, the following calculation path is used, as adapted from Schelten and Schmatz [12]. Given

$$S(q) = S_0 \frac{1}{1 + \frac{c_1}{a_2} q^2 + \frac{c_2}{a_2} q^4}, \tag{12}$$

the transform of the scattering function is

$$s(r) = \int_0^{\infty} J_0(qr) S(q)\, dq \tag{13}$$

and $s(r)$ yields $h(r)$, the transform of $H(q)$, according to

$$h(r) = k_0^2 e^{-s_0/k_0^2} \left(e^{s(r)/k_0^2} - 1\right). \tag{14}$$

$h(r)$ yields the multiple scattered intensity

$$H(q) = \frac{1}{2\pi} \int_0^{\infty} J_0(qr) h(r)\, dr. \tag{15}$$

$S(q)$ and $H(q)$ were evaluated using the experimental q values to directly compare $H(q)$ with the experimental spectra. Two parameters in the Teubner–Strey $S(q)$, c_1/a_2 and c_2/a_2, define the shape of the spectrum, while the prefactor, S_0, incorporates the parameter a_2 and describes the overall intensity. Since S_0 varies as $D\Delta\rho^2$, the relative changes in spectra due to multiple scattering caused by samples with varying thickness or scattering contrast can be calculated using the procedure above. The proportionality constant S_0, however, is not known a priori.

3.3. Absolute scale

One of the benefits of neutron scattering is the assignment of absolute scattering intensity through the use of appropriate standards. However, inspection of the scattering function for bicontinuous microemulsions (Eq. (5)) indicates that the absolute scale is not independent of one of the three fitted parameters, a_2. Therefore, the assignment of absolute scale is not independently determinable separate from the influence of the microstructure. This is made explicit when Eq. (5) is rearranged to Eq. (12), and the resulting form of the spectra is dependent on only two groups of parameters, c_1/a_2 and c_2/a_2. While these two fitted parameters set the microstructural properties d and ξ, a third independent parameter may

be chosen arbitrarily to set the scale of the model. Therefore, the absolute scale of bicontinuous microemulsion scattering can be dropped and fit with two parameters without any loss of microstructural information contained within the scattering spectra.

More generally, if the absolute scale of a model intensity, $S(q)$, were mathematically distinct from the fitted parameters, the formalism of Schelten and Schmatz does not explicitly account for any attenuation of the main neutron beam besides that due to coherent elastic scattering. For the model calculations to reflect the observed changes in attenuation in absolutely calibrated samples, the effect of all neutron–nucleus interactions must be treated explicitly in the parameter μ of Eq. (10). The cross section for every interaction of the incident neutrons with the sample nuclei as a function of sample composition is not available. In the absence of such information, the unknown attenuation factor due to all other processes besides small angle scattering becomes another fitted parameter that carries through the model calculation as an arbitrary factor that effectively sets the absolute scale.

For the model calculations of multiple scattering the following steps have been taken to remove the ambiguity behind the determination of absolute scale and attenuation. The model intensity I_{TS} is recast to depend on only two parameters which set the microstructure of the sample (Eq. (12)). As these are thermodynamic parameters, they are held constant when fitting multiple spectra with the same overall composition, but differing contrasts or path lengths. During fitting, the model intensity for each sample is rescaled arbitrarily to the experimental data at one q position for all spectra, namely, q position of the main peak in the 50% D_2O sample. This procedure removes the uncertainty associated with the assignment or measurement of a "scattering" transmission, allowing the change in coherent q-dependent scattering to be examined independently.

4. Results

Figure 1 shows the increase in surfactant efficiency caused by adding small amounts of cationic surfactant to a nonionic microemulsion. 2% DDAB in a surfactant mixture with C_8E_3 yields an decrease in the amount of surfactant needed to solubilize equal weights of decane and water from $\tilde{\gamma} = 23$ to $\tilde{\gamma} = 6$. The changes in phase behavior upon adding an ionic surfactant to a nonionic microemulsion and the concomitant changes in microstructure have been examined previously [19,23–26].

In SANS experiments, H_2O is usually replaced with D_2O to increase the coherent scattering cross section and decrease the amount of incoherent scattering. While the standard composition variables from microemulsion literature are designated by weight fraction, the small changes in volumetric composition caused by isotopic substitution are small. The most notable impact of systematic substitution of

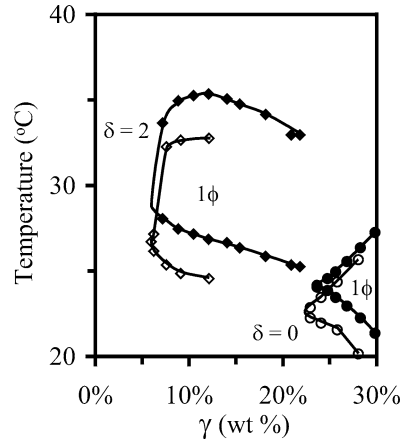

Fig. 1. Phase diagram of C_8E_3, DDAB, decane, and water at $\alpha = 50$ and $\delta = 0$, 2. Closed symbols represent phase boundaries in water, while open symbols represent phase boundaries in D_2O. Only the region where one-phase microemulsions form is displayed.

D_2O for H_2O is a change in the temperature of phase boundaries of a few degrees in Fig. 1. All SANS spectra reported in this paper were performed on solutions at $\gamma = 8$, $\alpha = 50$, $\delta = 2$, and $T = 27\,^{\circ}C$. The scattering contrast was varied by altering the amount of D_2O in the aqueous mixture (by weight) from 100% to 90%, 75%, and 52%. The change in water composition will cause slight temperature differences with respect to the location of the phase boundary, but all solutions were observed to be one phase at the compositions and temperature listed above. The change in microemulsion structure caused by isotopic substitution is assumed to be negligible compared to the effects of multiple scattering.

In addition to varying the D_2O composition, samples at 100% and 90% D_2O were both measured in cells with path lengths of 1 and 2 mm. The resulting six spectra (Fig. 2) are samples at 100% D_2O (1- and 2-mm path length), 90% D_2O (1- and 2-mm path length), 75% D_2O (1 mm), and 52% D_2O (1 mm). The experimentally measured transmissions for the solutions at 100% and 90% D_2O in the two cells are 27%, 8%, 30%, and 10%, respectively.

Figure 3 compares the scattering spectra from solutions at $\gamma = 8$, $\delta = 2$, and $T = 27\,^{\circ}C$ in 1- and 2-mm cells (see Fig. 1). Increasing the sample thickness from 1 to 2 mm causes the following changes in the scattering spectra: the main peak becomes broader, a secondary peak appears at $2q_{max}$, and the background scattering increases dramatically. Since the only difference between the two samples is the sample thickness, all of these effects are due to the larger scattering probability in the thicker sample. The inset shows the data as Iq^4 vs q on a linear scale. Simple microemulsion scattering should yield one peak and a straight line at higher q, yet both spectra indicate two peaks and distinctly higher intensity at higher q.

Figure 4 illustrates the problems of a least-squares fit of the Teubner–Strey model to the 1-mm, 100% D_2O sample data. When trying to fit the entire q range, the model fails to fit the main scattering peak at q_{max} and significant

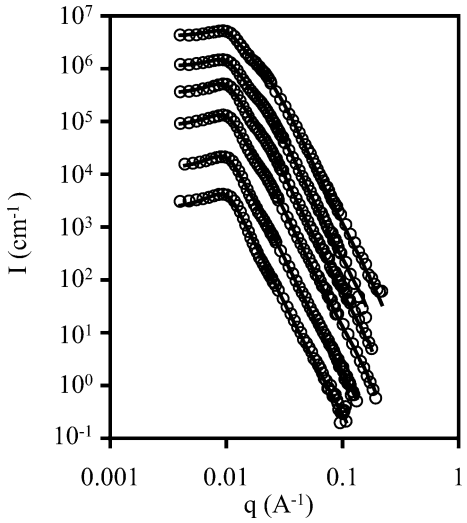

Fig. 2. SANS spectra of C_8E_3, DDAB, decane, and water at $\gamma = 8$, $\alpha = 50$, $\delta = 2$, and $T = 27\,^{\circ}\mathrm{C}$. The spectra from bottom to top are from samples with 1 mm path lengths and weight fractions of D_2O of 0.52, 0.75, 0.90, and 1, and 2 mm path lengths and weight fractions of D_2O of 0.90 and 1. Subsequent curves are offset for clarity. The solid lines are the fit of the multiply scattered Teubner–Strey model.

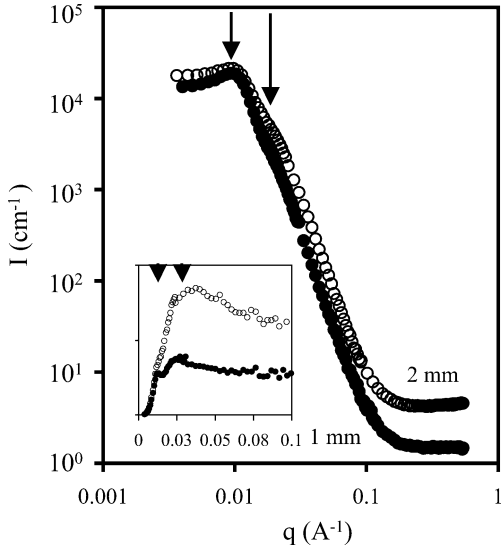

Fig. 3. SANS spectra of C_8E_3, DDAB, decane, and D_2O at $\gamma = 8$, $\alpha = 50$, $\delta = 2$, and $T = 27\,^{\circ}\mathrm{C}$ with 1- and 2-mm path length. Arrows denote the q-positions of the main peak, $q_{\max}$, and twice the main peak, $2q_{\max}$. Inset shows the same data as Iq^4 vs q on a linear scale to emphasize the secondary peak in the scattered intensity. Background has not been subtracted to demonstrate differences in intensity.

deviations are present around $2q_{\max}$. The inset shows the same data as Iq^4 vs q on a linear scale. The results for fitting I_{TS} to the entire q range are reported in Table 1 with χ^2 values. Since previous authors have reported the results of fitting I_{TS} to only the peaks of the spectra [9], Fig. 5 shows the results of fitting just the scattering peaks to I_{TS} for samples with varying contrast and thicknesses but at the same overall composition. The resulting model parameters are reported in Table 1, along with χ^2 values for

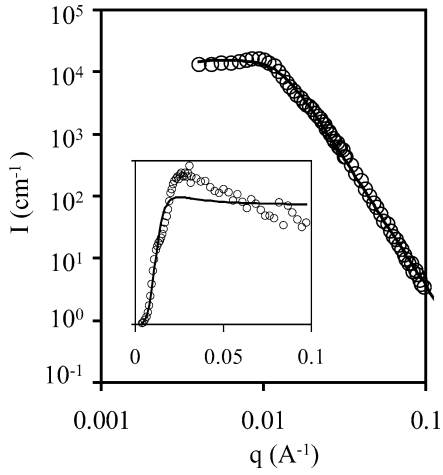

Fig. 4. Typical data and model fit using the Teubner–Strey model over the entire q-range. Significant errors are present in the low q portion of the spectra. Inset shows Iq^4 vs q on a linear scale. Parameters for each fit are reported in Table 1.

the various fits. The fitted values of the model parameters change systematically, and the apparent values of the domain spacing and correlation length decrease with higher contrasts and thicknesses. These changes simply reflect differing amounts of multiple scattering in the spectra.

5. Discussion

Figure 3 shows the prominent changes in scattering spectra for strongly scattering bicontinuous microemulsions due to changes in sample thickness. Since the sample compositions are identical and the spectra are normalized for sample thickness when placed on absolute scale, these two spectra should overlap completely. However, for the thicker sample there is increased intensity at low q, a widening of the main peak, increased intensity at twice the q value of the main peak, $2q_{\max}$, and a higher background. Data from transmission files indicate that the upturn at low q blends smoothly into the profile of the transmitted beam, suggesting that broadening of the beam might be responsible for this effect. The width of the main peak is obviously larger in the 2-mm sample than the 1-mm sample due to the tendency of multiple scattering to smear higher intensities, and thus blunt the peak shape. The increased scattering at $2q_{\max}$ is the most prominent change in the shape of the spectra and is due to double imaging of the main scattering peak, i.e., multiple scattering of neutrons from the main peak. This is shown most prominently in the inset of Iq^4 vs q. The two arrows point to the q positions of the main correlation peak and $2q_{\max}$. The background, arising mainly from incoherent scattering, increases with the thickness of the sample due to the increase in overall scattering probability. With a series of spectra as shown here, the presence of a secondary peak is clearly identifiable as an effect of multiple scattering.

Table 1
Results from Teubner–Strey model fits of six SANS spectra using the full q-range, the initial q-range, and the full q-range incorporating multiple scattering effects

$\Delta\rho/\Delta\rho_{max}$	D	$D\Delta\rho^2$	Full q-range				0–2q_{max}				Full q-range—multiply scattered			
	(mm)	(normalized)	χ^2	ξ (Å)	d (Å)	f_a	χ^2	ξ (Å)	d (Å)	f_a	χ^2	ξ (Å)	d (Å)	f_a
0.49	1	0.12	42	243	639	−0.70	78	252	638	−0.72	67	260	646	−0.73
0.72	1	0.26	47	204	634	−0.61	23	238	630	−0.70	40	260	646	−0.73
0.89	1	0.40	73	185	631	−0.54	26	228	628	−0.68	33	260	646	−0.73
1.00	1	0.50	89	167	625	−0.48	48	216	619	−0.66	31	260	646	−0.73
0.89	2	0.79	80	129	628	−0.25	49	175	617	−0.52	14	260	646	−0.73
1.00	2	1.00	99	110	613	−0.12	69	157	600	−0.46	26	260	646	−0.73

Note. Samples are identified by their path length and relative contrast (varied by H_2O/D_2O ratio). χ^2 values are also included to indicate relative accuracy of each description.

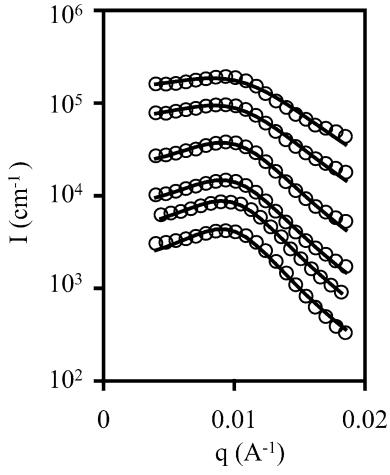

Fig. 5. Data and model fits using the Teubner–Strey model over the q-range up to $2q_{max}$. Parameters for each fit are reported in Table 1 and Fig. 6. The spectra from bottom to top are from samples with 1 mm path lengths and weight fractions of D_2O of 0.52, 0.75, 0.90, and 1, and 2 mm path lengths and weight fractions of D_2O of 0.90 and 1.

Proceeding with the normal course of data treatment involves the subtraction of background scattering to leave data similar to that displayed in Fig. 4. Attempting to fit this data with the Teubner–Strey model over the entire q range yields the solid line. The main peak is fit poorly, mostly due to the increase in scattering observed at and above $2q_{max}$. The inset of Iq^4 vs q indicates that the model fit interpolates between the two peaks in the scattering spectra while fitting neither. To quantitate the quality of fit, χ^2 values for the entire q range are reported in Table 1. All of these indicate what can be detected visually, namely, that the I_{TS} functional form is unable to reproduce data of the type displayed in Fig. 3. In addition, the magnitude of χ^2 increases with both the thickness and scattering contrast, indicating multiple scattering systematically affects the ability of I_{TS} to reproduce the experimental data.

To understand how multiple scattering can affect the quality of data derived from fitting just the peak in the scattering data, the results for fitting the initial q range (from q_{min} to $2q_{max}$) are displayed in Fig. 5 and Table 1. Between the spectra for samples with the smallest and largest contrasts and thicknesses, variations of 6%, 38%, and 36% are detected in d, ξ, and f_a, respectively. In addition, one is never confident that even the sample measured at the smallest contrast and thickness is devoid of multiple scattering, indicating somewhat larger variations between those measured and the "true" microstructural parameters. The persistence length is obviously the parameter most affected by multiple scattering, as might be expected due to the smearing of the main intensity peak and the relative increase of its width at half maximum. However, the change in domain size is also substantial. The apparent value of the amphiphilicity factor, which is derived from the other two parameters, is increased by the change in scattering power, indicating, incorrectly, that the strongly scattering solutions are significantly less organized than they actually are. Table 1 reports that the reduction in q range results in lower χ^2 values for the I_{TS} fits, as might be expected from arbitrarily trimming the scattering data. The magnitude of χ^2 generally increases as the thickness and contrast increase, as did the χ^2 values for fits to the full range of q. This indicates a correlation between the quality of fit and the experimental parameters controlling the scattering power of the solutions.

The multiple scattering component of these spectra must be determined to quantify and correlate the trends in I_{TS} parameters. Since multiple scattering is related to the overall intensity (or scattering probability), it is reasonable that it might also scale with the experimental parameters D and $\Delta\rho^2$. Figure 6 shows that the values of d and ξ correlate linearly with the product $D\Delta\rho^2$, indicating that the isotopic substitution of water is not systematically skewing the scattering spectra. The linear regressions for the values for d and ξ can be rearranged to obtain the values of f_a, shown in the third panel of Fig. 6. Extrapolating these regressions to $D\Delta\rho^2 \to 0$ yields values of $d = 641$ Å, $\xi = 268$ Å, and $f_a = -0.75$ for this sample. The intercepts should be good approximations for the "true" values for the microstructural parameters for a singly scattered solution. Thus, an experiment using a few samples of varying thickness or contrast can be used to obtain estimates for the microstructural parameters of strongly scattering microemulsions.

The microstructural values obtained by extrapolation should also be obtainable from the multiply scattered spec-

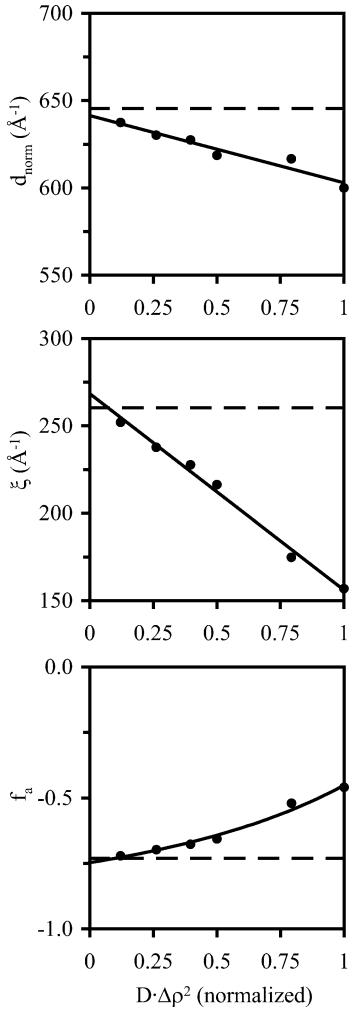

Fig. 6. Domain spacing, d, correlation length, ξ, and amphiphilicity factor, f_a, for Teubner–Strey model fits over the initial q-range plotted against $D\Delta\rho^2$ normalized to the largest path length and contrast. Solid lines indicate linear extrapolations to zero $D\Delta\rho^2$, while dashed lines are values obtained from the multiple scattering analysis explained in the text.

tra themselves by accounting for the multiple scattering using the method of Schelten and Schmatz [12]. Several approaches can be taken to extract a consistent set of d and ξ values from the six experimental spectra. Here, two data sets are used to determine d and ξ, while the other four are interpolated to examine how the model handles the scaling of multiple scattering effects. The numerical procedure of Eqs. (12)–(15) is used to calculate the multiply scattered version of I_{TS} as a function of d and ξ. As the absolute amount of multiple scattering is not known, one value of S_0 is allowed to vary in the model fitting. Subsequently, the relative values of S_0 for each data set are set by the sample composition and path length.

The most and least multiply scattered spectra (100% D_2O, 2 mm, and 52% D_2O, 1 mm) are fit simultaneously to determine a single set of parameters for both data sets; $d = 646$ Å, $\xi = 260$ Å. Once the absolute value of S_0 is determined, all the remaining model data sets were directly

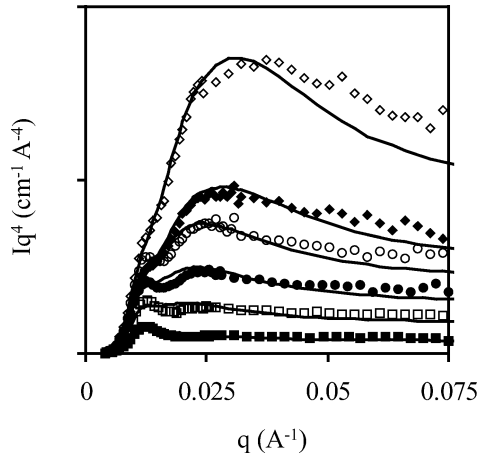

Fig. 7. SANS spectra of Fig. 2 plotted as Iq^4 vs q on a linear scale. The lines are from the multiply scattered Teubner–Strey model. The top and bottom spectra were fit simultaneously, while the remaining four spectra were interpolated using the values of D and $\Delta\rho^2$.

calculated using the same I_{TS} parameters and the scaling of S_0 by $D\Delta\rho^2$. Thus, two data sets are fit with the numerical procedure, while the other four are interpolated.

Figures 2 and 7 show the resulting model spectra with the experimental data on a log scale and as Iq^4 vs q, respectively, with each spectra offset for clarity. The top and bottom spectra were fit simultaneously, while the middle spectra were extrapolated. The procedure of Schelten and Schmatz allows the interpretation of many of the experimental "artifacts" contained within the data. Notably, the peak at $2q_{max}$ scales with the scattering power of the solutions. Similarly, the peak width increases with multiple scattering, while the value of ξ remains constant throughout the model fits. The parameters derived from the multiple scattering model fit are displayed as dashed lines in Fig. 6 and independently corroborate the extrapolations to zero scattering power discussed earlier. The χ^2 values from the multiple scattering procedure are generally equal to or less than those for fitting the main peak to I_{TS}. This is despite the fact that only two of the data sets are included in the fitting process, the entire q range is utilized instead of just a subset, and the number of fitted parameters over the six data sets is 3 instead of 12. Therefore, the calculation path introduced by Schelten and Schmatz [12] successfully describes the changes in spectra from bicontinuous microemulsions under the conditions of multiple scattering.

6. Summary

SANS spectra from efficient microemulsions likely contain at least some amount of multiple scattering, especially as the microstructure becomes correlated over longer distances. The characteristic effects of multiple scattering include an increase in low q scattering, an increase in the width of any scattering peaks, a multiple image of the main scattering peak, and an increase in background scattering. Mea-

surement of solutions at differing contrasts and thicknesses show a linear dependence of d and ξ on the scattering probability. Extrapolation of these parameters to zero thickness or contrast provides good estimates for the actual microstructural parameters. This extrapolation was corroborated by simultaneously fitting multiple scattering curves utilizing the procedure of Schelten and Schmatz [12] to account for multiple scattering. The results produce a consistent set of parameters that apply to all the solutions measured.

Acknowledgments

We are grateful for research support from Dow Corning. We acknowledge the support of the National Institute of Standards and Technology, U.S. Department of Commerce, in providing facilities used in this work.

References

[1] M.E. Cates, S.A. Safran, Curr. Opin. Colloid Interface Sci. 2 (1997) 359.
[2] K. Holmberg, R. Laughlin, Curr. Opin. Colloid Interface Sci. 2 (1997) 453.
[3] M. Teubner, R. Strey, J. Chem. Phys. 87 (1987) 3195.
[4] O. Glatter, G. Fritz, H. Lindner, J. Brunner-Popela, R. Mittelbach, R. Strey, S.U. Egelhaaf, Langmuir 16 (2000) 8692.
[5] M. Gradzielski, D. Langevin, L. Magid, R. Strey, J. Phys. Chem. 99 (1995) 13232.
[6] H. Bagger-Jörgensen, U. Olsson, K. Mortensen, Langmuir 13 (1997) 1413.
[7] A. Bumajdad, J. Eastoe, P. Griffiths, D.C. Steytler, R.K. Heenan, J.R. Lu, P. Timmins, Langmuir 15 (1999) 5271.
[8] M. Gradzielski, D. Langevin, B. Farago, Phys. Rev. E 53 (1996) 3900.
[9] T. Sottmann, R. Strey, S.H. Chen, J. Chem. Phys. 106 (1997) 6483.
[10] H.S. Snyder, W.T. Scott, Phys. Rev. 76 (1949) 220.
[11] H.A. Bethe, Phys. Rev. 89 (1953) 1256.
[12] J. Schelten, W. Schmatz, J. Appl. Crystallogr. 13 (1980) 385.
[13] N.F. Berk, K.A. Hardman-Rhyne, J. Appl. Crystallogr. 21 (1988) 645.
[14] M. Monkenbusch, J. Appl. Crystallogr. 24 (1991) 955.
[15] P.S. Goyal, J.S. King, G.C. Summerfield, Polymer 24 (1983) 131.
[16] S. Mazumder, A. Sequeira, J. Appl. Crystallogr. 25 (1992) 221.
[17] A.L. Barabanov, S.T. Belyaev, Eur. Phys. J. B 15 (2000) 59.
[18] M. Kahlweit, R. Strey, Angew. Chem. Int. Ed. Engl. 24 (1985) 654.
[19] M. Kahlweit, R. Strey, J. Phys. Chem. 92 (1988) 1557.
[20] O. Glatter, O. Kratky, in: Small Angle X-Ray Scattering, Academic Press, New York, 1982, p. 515.
[21] K.-V. Schubert, R. Strey, J. Chem. Phys. 95 (1991) 8532.
[22] K.-V. Schubert, R. Strey, S.R. Kline, E.W. Kaler, J. Chem. Phys. 101 (1994) 5343.
[23] H. Kunieda, K. Hanno, S. Yamaguchi, K. Shinoda, J. Colloid Interface Sci. 107 (1985) 129.
[24] M. Kahlweit, B. Faulhaber, G. Busse, Langmuir 10 (1994) 2528.
[25] L.D. Ryan, E.W. Kaler, J. Phys. Chem. 102 (1998) 7549.
[26] J.A. Silas, E.W. Kaler, R.M. Hill, Langmuir 17 (2001) 4534.